Open access • Posted Content • DOI:10.1101/2020.06.16.154609

Wnt- and Glutamate-receptors orchestrate stem cell dynamics and asymmetric cell division — Source link

Sergi Junyent, Joshua Reeves, James L. A. Szczerkowski, Clare L. Garcin ...+3 more authors

Institutions: King's College London

Published on: 16 Jun 2020 - bioRxiv (Cold Spring Harbor Laboratory)

Topics: Wnt signaling pathway, LRP6, Asymmetric cell division, LRP5 and Cell fate determination

Wnt- and Glutamate-receptors orchestrate stem cell dynamics and asymmetric cell division

Sergi Junyent*,[1], Joshua Reeves*,[1], James L. A. Szczerkowski[1], Clare L. Garcin[1], Tung-Jui Trieu[1], Matthew Wilson[1] and Shukry J. Habib#,[1]

*These authors contributed equally

#Correspondence to: shukry.habib@kcl.ac.uk

[1]Centre for Stem Cells and Regenerative Medicine, King's College London. 28th Floor, Tower Wing, Guy's Campus, Great Maze Pond, SE1 9RT. London, United Kingdom.

ABSTRACT

Wnt signalling regulates many aspects of cell biology. Wnt-pathway activation and its downstream effects have been extensively studied, but the dynamic analysis of Wnt-ligands on mammalian cellular membranes is obstructed by difficulties of visualization. We overcome this using microbead-tethered Wnts presented to single embryonic stem cells, which undergo Wnt-mediated asymmetric cell division (ACD). Through live imaging and genetic editing, we show that knockout of Wnt co-receptor Lrp5 promotes cytoneme formation and Wnt-recruitment, which requires Lrp6 and β-catenin. Lrp5 facilitates ligand-retention at the membrane, and alongside Lrp6 mediates Wnt-ligand stabilization and positioning. β-catenin or Wnt co-receptor knockout causes misorientation at mitosis, and all but Lrp5 are required for Wnt-orientated ACD. Surprisingly, ionotropic glutamate receptor (iGluR) activity enables initial Wnt-recruitment, positioning, and ultimately oriented ACD. Uniquely, we have scrutinized the early Wnt ligand-membrane interaction, linking roles of Wnt-pathway components and crosstalk with iGluRs in guiding cell fate determination by oriented ACD.

INTRODUCTION

Wnt signalling is an ancient pathway that accompanied the evolution of metazoans and plays major roles in cell biology, development, tissue homeostasis and disease (Clevers, 2006; Garcin and Habib, 2017). This pathway is regulated by Wnt ligands, which are palmitoylated in the endoplasmic reticulum (Takada et al., 2006). The lipid moiety is crucial for Wnt secretion and renders the protein hydrophobic (Willert et al., 2003). Consequently, Wnts are often secreted locally by producing cells (Langton et al., 2016; Mills et al., 2017). Wnt ligand binding to the receptor Frizzled (Fzd) and the co-receptors Low-density lipoprotein receptor-related protein 5 and 6 (Lrp5 and Lrp6) leads to the initiation of a signalling cascade that results in the stabilization of β-catenin, its nuclear translocation and the transcription of Wnt/β-catenin target genes (Nusse and Clevers, 2017).

Concomitantly, Wnt signalling can control the morpho-kinetics of the receiving cells, often involving a crosstalk with β-catenin independent signalling cascades (James et al., 2008; Komiya and Habas, 2008). As a result, Wnt reception can initiate a complex signalling program that coordinates cell cycle progression (Niehrs and Acebron, 2012), cytoskeleton arrangement (Salinas, 2007; Stamatakou et al., 2015), cell migration (Sedgwick and D'Souza-Schorey, 2016) and cell polarization (Goldstein et al., 2006; Stanganello et al., 2019). In stem cells, localized Wnt activity controls cell fate by inducing self-renewal and blocking differentiation (Clevers et al., 2014; Garcin and Habib, 2017).

Components of the Wnt signalling pathway modulate many aspects of the mitotic program, including microtubule dynamics, spindle formation and centrosome division (Niehrs and Acebron, 2012). Lrp6 is phosphorylated at G2-M, which enhances Wnt signalling in a cell cycle-dependent manner (Davidson et al., 2009), and Fzd and Lrp6 establish spindle orientation and promote mitotic progression in HeLaS3 cell line (Kikuchi et al., 2010). β-catenin accumulates at the centrosomes, and regulates radial microtubules and centrosome splitting (Bahmanyar et al., 2008; Huang et al., 2007). These reports and others (Akong et al., 2002; Bienz, 2005; Hendriksen et al., 2008; McCartney et al., 1999; Mizumoto and Sawa, 2007; Tahinci et al., 2007) suggest a role for the intrinsic Wnt pathway components in the regulation of cell polarization and cell division. *In vivo* studies in non-mammalian systems (*C. elegans*, *Drosophila* and *Xenopus*) have also demonstrated that localized Wnt reception influences cell fate by inducing oriented asymmetric cell division (ACD) (Bertrand, 2016; Goldstein et al., 2006; Huang and Niehrs, 2014; Kaur et al., 2020; Sugioka et al., 2011; Walston et al., 2004).

In these systems, the coordinated effects of Wnt activation arise from the interaction between localized Wnt ligands and Wnt pathway components at the cell membrane.

However, our understanding of localized Wnt recognition in mammalian cells remains elusive. Insights into Wnt ligand-receptor interaction so far has been restricted to genetic and/or biochemical analysis, or transcription of target genes (Mills et al., 2017). *In vitro* studies have often relied on the addition of solubilized Wnt ligands to the media, which does not recapitulate the localized presentation of Wnt often observed *in vivo* (Garcin and Habib, 2017; Mills et al., 2017). Moreover, direct tagging and visualization of mammalian Wnt proteins has proven difficult (Willert and Nusse, 2012), which complicates the study of the effects of Wnt at the single cell level. As a result, the molecular events that control Wnt reception and kinetics in the cell remain elusive.

To overcome these issues, we previously developed a system of localized Wnt presentation to study Wnt response at the single cell level. We covalently immobilized biologically active Wnt ligands to microbeads, generating a source of localized Wnt (a Wnt-bead) that can be visualized by light microscopy and tracked over time (Habib et al., 2013; Lowndes et al., 2017). We employed this approach to study the effect of localized Wnt signals on stem cells.

Embryonic stem cells (ESCs) are a powerful tool to investigate cell fate. ESCs are Wnt responsive (ten Berge et al., 2011) and can be seeded as single cells and retain the capacity to self-renew and differentiate to all lineages of the adult body (Martello and Smith, 2014). Additionally, recent data reveals that in ESCs, Wnt reception and the subsequent activation of the Wnt/β-catenin pathway act independently of receptor internalization (Rim et al., 2020). By combining the Wnt-beads with live cell imaging at high temporal resolution we observed that ESCs generate specialized membrane protrusions, termed cytonemes, that recruit localized Wnt signals. This recruitment is mediated by a crosstalk between Lrp6 and ionotropic glutamate receptor (iGluR) activity (Junyent et al., 2020). Wnt-bead recruitment initiates a polarization event involving components of the Wnt/β-catenin pathway, orients the mitotic spindle and leads to ACD (Habib et al., 2013; Junyent et al., 2020). This results in a Wnt-bead proximal cell that maintains high levels of pluripotency markers (*e.g.* Nanog, Rex1), and a Wnt-bead distal cell that progresses to a more differentiated cell fate (Habib et al., 2013). However, the molecular mechanisms underpinning this process also remained understudied.

Here, we combine Wnt-beads with genetic editing of ESCs to investigate the kinetics of Wnt reception. We interrogate how intrinsic components of the Wnt pathway control the cellular response to localized Wnts that leads to ACD. We used ESCs knock-out (KO) for the Wnt co-receptors Lrp5, Lrp6 and a double Lrp5/6 KO to dissect the role of the early reception complex in Wnt ligand interaction and response (Junyent et al., 2020). We also studied an inducible β-catenin KO ESC line that enables rapid ablation of protein without long term

compensation effects (Raggioli et al., 2014) to investigate the role of the downstream effector of the Wnt/β-catenin pathway. Moreover, we pharmacologically inhibit the activity of iGluRs to examine how crosstalk between Wnt reception and iGluRs modify the cell response to localized Wnt signals beyond initial ligand recognition.

Our time-series analysis resolves the dynamics of Wnt ligand recruitment by single ESCs into three stages: initial cytoneme-mediated interaction, early Wnt interaction with the cell membrane, and the subsequent effects of the Wnt-bead recruitment on spindle orientation and cell fate choice. We show that Lrp6, iGluR activity and β-catenin are required for the recruitment of the Wnt beads to the cell. On the other hand, KO of Lrp5 promotes cytoneme generation and facilitates Wnt-bead recruitment. Co-receptor or β-catenin KO, or inhibition of iGluR, restricts Wnt-bead position to the periphery of the cell. KO of Lrp5 or Lrp6 leads to increased Wnt bead movement, and ESCs lacking Lrp5 maintain Wnt-bead contact for shorter times. Upon progression to mitosis, co-receptor or β-catenin KO, or iGluR inhibition, impairs spindle orientation. Only Lrp5KO ESCs retain the capacity to asymmetrically partition pluripotency markers between daughter cells.

Altogether, our data explores how Wnt receptors, β-catenin and the activity of iGluRs orchestrate the dynamics of a stem cell interaction with localized Wnt signals, and how these components subsequently regulate asymmetric cell division.

RESULTS

The Wnt co-receptor Lrp6 regulates the prevalence and rate of cytoneme formation of ESCs

We aimed to investigate how components of the Wnt/β-catenin pathway affect the cellular dynamics of ESCs and their capacity to respond to Wnt ligands. To do so, we used our previously published knock-out (KO) ESC lines. We KO the co-receptors of the Wnt/β-catenin pathway Lrp5 (Lrp5KO), Lrp6 (Lrp6KO) and generated a double KO of both Lrp5 and 6 (Lrp5/6dKO) in mouse embryonic stem cells (ESCs), as previously described (Junyent et al., 2020) (**Fig. 1A**). We also utilized an ESC line with a conditional KO of the effector of the pathway, β-catenin (βKO), which was generated as previously described (Junyent et al., 2020; Raggioli et al., 2014). In this line, complete β-catenin depletion is achieved after 3-day induction with 4-hydroxytamoxifen (4-HT).

We validated the response of the KO cell lines to exogenous Wnt3a ligands. We used cell lines harbouring a reporter of the transcriptional co-activator activity of β-catenin, which express eGFP upon β-catenin-Tcf/Lef binding its 7xTCF promoter (Fuerer and Nusse, 2010) (**Fig. 1B**). In the presence of purified Wnt3a ligands and serum containing media, 49.06% of wild-type (WT) cells express eGFP (**Fig. 1B and C**). In the absence of Wnt3a, only a basal level of pathway activation is observed. Lrp5KO ESCs, when stimulated with Wnt3a, have a significant reduction in activation of the Wnt/β-catenin pathway in comparison to WT ESCs (26.96% $eGFP^+$ cells). In Lrp6KO ESCs, pathway activation is further compromised (5.60% $eGFP^+$ cells). Lrp5/6dKO ESCs cannot activate the Wnt/β-catenin pathway at all by soluble Wnt3a stimulation. βKO, which lacks β-catenin expression, also does not activate the pathway during Wnt3a stimulation.

To facilitate expansion of the cell lines, we cultured cells in 2i media (CHIR 99021, PD0325901) that maintains ESC self-renewal without the requirement for Wnt ligands or Wnt-receptor activity (Ying et al., 2008). Under these conditions, receptor KO ESCs maintain levels of pluripotency markers comparable to those of WT cells. The conditional β-catenin KO cell line has reduced levels of pluripotency markers after 3-day induction with 4-HT, compared to the WT cells (Junyent et al., 2020). In all performed experiments, cell lines were seeded as single cells at low density in a serum-containing media without 2i.

ESCs utilize cytonemes to recruit Wnt ligands immobilized to a microbead (Wnt3a-beads) (Junyent et al., 2020). We have previously reported (Junyent et al., 2020) that at the single cell level, WT ESCs produce an average of 5 cytonemes that extend to an average maximum length of 29.9 μm (also depicted in **Fig. 1D, Movie 1**). The KO ESC lines exhibit variability in the average number of cytonemes per cell, between 4 for co-receptor KOs

(**Movie 2-4**) and 7 for βKO (**Movie 5**). Cytoneme length is shorter in KO ESCs than in WT cells, with an average maximum length of 16.3 - 23.0 μm for coreceptor KOs, and ~20.0 for βKO (**Fig 1D**). Regardless of differences in cytoneme characteristics, all ESC lines studied use cytonemes in a similar way to facilitate interaction with the surrounding environment (Junyent et al., 2020).

To investigate whether KO of Wnt/β-catenin pathway components affects the dynamics of cytoneme formation in ESCs, live imaging was performed. Single cells were seeded at low density and imaged for 12 hours. Measurement of the percentage of cells with cytonemes revealed that WT ESCs begin forming cytonemes upon substrate attachment. Within 4 hours, over 40% of WT ESCs had cytonemes (**Fig. 1E**). Interestingly, more Lrp5KO ESCs generate cytonemes than WT ESCs, reaching 55.53% in 3 hours. The rate of increase in the percentage of cells with cytonemes is similar to WT in Lrp6KO and βKO, with the percentage of cells with cytonemes in Lrp5/6dKO cells being slightly reduced, and plateauing marginally, but significantly, lower at 31.83%.

Together with cytoneme formation, cell motility provides a mechanism to encounter and interact with the local environment. To understand whether the observed changes in the cytonemes of the Wnt/β-catenin pathway KOs are coupled with changes to their movement, we tracked the position of the cell over time. The Mean Squared Displacement (MSD), the measure of the average cell movement per minute, revealed that cell motility in WT ESCs is minimal, with an average MSD of 1.16 μm^2/min (**Fig. 1F**). No significant differences to WT were observed between receptor or β-catenin KO ESCs, with the average MSD values for each cell type falling between 0.97 and 1.49 μm^2/min.

Altogether, we observed that intrinsic Wnt/β-catenin components control the generation of cytonemes, without affecting overall cellular motility. Since ESCs use cytonemes to recruit localized Wnt signals, we aimed to further investigate how different components of the Wnt/β-catenin pathway affect the recruitment of Wnt3a-beads to the cell membrane.

Wnt co-receptors and iGluR activity orchestrate the interaction dynamics between localized Wnt3a and the ESC membrane

To examine the effect of Wnt/β-catenin pathway KOs on the capacity of ESCs to recruit localized Wnt signals, we seeded cells at low density and presented them with dispersed Wnt3a-beads. In some conditions, cells were presented with inactivated Wnt3a-beads (iWnt3a-beads), which are dithiothreitol (DTT)-treated to denature the Wnt3a protein while covalently bound to the bead. Cells were live-imaged each minute for a total of 12 hours.

We aimed to quantify the role of the co-receptors and β-catenin in the dynamics of the recruitment of localized Wnt3a to ESCs, integrating analysis at both the population and single cell level. This allowed us to quantify the capability of ESCs to form and maintain stable interactions with a source of localized Wnt3a, which can impact downstream cellular responses. To do so, we combined two measurements: Firstly, the proportion of cells which were in contact with a Wnt3a-bead over time was measured every hour from the start of the imaging for 12 hours (**Fig. 2A and B**). Secondly, contact between ESC and Wnt3a-bead was measured by the duration of a single cell-bead interaction (**Fig. 2A, C and D**).

At the population level, when WT cells were presented with Wnt3a-beads, the proportion of cells with beads increased linearly in the first 4 hours, rising from 20.68% at the beginning of the video to 56.73%, before rising more slowly to 66.75% after 12 hours (**Fig. 2B**). ESC cytonemes are ligand-selective and can efficiently recruit localized Wnt3a signals but not iWnt3a-beads (Junyent et al., 2020). Indeed, when WT ESCs are presented with iWnt3a-beads, the percentage of cells with beads does not rise and remains less than 20% for most of the time period (**Fig. 2B**). In terms of duration of interaction with the localized Wnt3a source, WT cells were found to retain Wnt3a-beads for over 380 minutes, on average. Many cells retained Wnt3a-beads until the end of the video (12 hours, **Fig. 2C-D**). iWnt3a-beads, however, are retained for a significantly shorter time (**Fig. 2D**). In this condition, iWnt3a-beads are often dropped after a shorter period (<60 minutes), showing as a more 'fragmented' plot (**Fig. 2C**).

ESCs lacking Lrp6 (Lrp6KO, Lrp5/6dKO) were impaired for Wnt3a-bead accumulation, similar to WT cells with iWnt3a-beads (**Fig. 2B**). The proportion of cells with beads does not rise, remaining at approximately 30% over the course of 12 hours (**Fig. 2B**). Lrp5KO cells retain the ability to accumulate Wnt3a-beads, reaching 55.86% after 5 hours (**Fig. 2B**). Cells lacking Lrp5 (Lrp5KO, Lrp5/6dKO) maintained contact with Wnt3a-beads for a significantly shorter time, frequently losing contact after 200 minutes. The contact duration of Lrp6KO cells with Wnt3a-beads was not significantly different to WT (**Fig. 2D**).

β-catenin ablation does not affect the reactivity of ESCs to a source of localized Wnt3a, when presented at a similar distance to WT cells (Junyent et al., 2020). However, similarly to Lrp6KO, cells lacking β-catenin (βKO) had significantly impaired Wnt3a-bead accumulation (**Fig. 2B**). Duration of localized Wnt3a contact, however, was not significantly different than WT (**Fig. 2C and D**).

A crosstalk between Lrp6 and the activity of AMPA/Kainate glutamate receptors (iGluRs) regulates the reactivity of ESC cytonemes to Wnt3a beads (Junyent et al., 2020). Here we show that pharmacological inhibition of iGluRs by cyanquixaline (CNQX) in WT ESCs did not

affect the rate of cytoneme formation or the cell movement (**Fig. 1E and F**). However, the percentage of cells with beads was significantly lower during CNQX inhibition than untreated WT ESCs, despite similar retention time of the Wnt3a-bead (**Fig. 2B-D**).

Differences in the retention time and proportion of cells with Wnt3a-beads between Lrp5KO and Lrp6KO demonstrates that components of the Wnt/β-catenin pathway have different roles in the overall process of signal reception. Further, the differing effects of receptor or effector KOs show that stable signal recruitment is a combination of several cell-signal processes. While Lrp6, β-catenin, and activity of iGluRs are required for the efficient uptake and accumulation of Wnt3a-beads, Lrp5 regulates the stability of the interaction.

Despite these differences, it is important to note that cells of all types and in all conditions do uptake Wnt3a-beads, allowing further analysis of the interaction with localized Wnt3a. As the recruitment is the first stage of many in the process of signal reception, we aimed to investigate the dynamics of the cell-bead contact during this interaction.

Lrp5 and Lrp6 have important but distinct roles in the positioning and stabilization of Wnt3a ligands on the ESC membrane

The Wnt3a-bead approach provides a unique opportunity to visualize and explore the dynamics of localized Wnt on the cell membrane. Therefore, we next studied the interaction between Wnt and cells after the initial Wnt3a-bead recruitment. To do so, we measured the Wnt-bead position at every minute after initial Wnt-bead recruitment, for 3 hours. To quantify the dynamics and location of Wnt3a-bead on the ESC membrane, we measured the distance between Wnt-bead and the cell centre, and we reported it as a proportion of the cell radius (**Fig. 3A**).

Cells recruit Wnt-beads to the cell membrane via cytonemes, where they initially reside in the periphery. WT ESCs rapidly pull the active Wnt3a-beads from the tip of the cytoneme, first to the periphery (between 0.7 and 1.0 of the cell radius), then closer in the cell body (between 0.3 and 0.7 of the cell radius). Within 1 hour, the Wnt3a-beads on average were between 0.5 and 0.6 of the cell radius, indicating close contact with the central portion of the cell body (**Fig. 3A-C**). iWnt3a-beads are recruited by WT ESCs less frequently (**Fig. 2B**) (Junyent et al., 2020). If recruited, iWnt3a-beads are also initially moved from the cytoneme tip to the periphery (0.7 to 1.0 of the cell radius). However, iWnt3a-beads are not positioned further within the cell body, reaching at closest 0.7 of the cell radius, on average (**Fig. 3A-C**).

ESCs lacking Lrp6 (Lrp6KO, Lrp5/6dKO) are likewise, on average, unable to recruit the Wnt3a-bead closer to the cell body (**Fig. 3B-C**). After approximately 150 minutes Lrp5KO ESCs are able to position the bead to within 0.6 of the cell radius, however this remains

significantly impaired when compared to the WT cells. ESCs lacking β-catenin, or WT ESCs during CNQX inhibition, are also unable to maintain the bead closer than 0.7 of the cell radius (**Fig. 3B-C**).

KO of the receptors of the Wnt/β-catenin pathway, ablation of β-catenin, or inhibition of iGluR activity results in the significantly impaired prolonged positioning of a source of localized Wnt3a after recruitment by ESC cytoneme. Our data demonstrates differences in the positioning of the Wnt3a-bead relative to the cell, however the dynamics of the Wnt3a-cell interaction are also defined by the motion of the Wnt3a-bead relative to the cell. This led us to investigate the movement of the bead on the membrane. We calculated the MSD of the bead relative to the centre of the nucleus, for each frame of the same sequence of images as the bead position measurements (**Fig. 3D**).

Our analysis indicates that iWnt3a-beads held by WT ESCs have a higher rate of movement than Wnt3a-beads, with an average MSD of 5.09 μm^2/min, compared to 3.33 μm^2/min for Wnt3a-beads (**Fig. 3E**). The Wnt3a-beads on ESCs lacking Lrp5 (Lrp5KO), Lrp6 (Lrp6KO) or the Lrp5/6dKO have a MSD significantly higher, at 4.76 μm^2/min, 4.89 μm^2/min and 4.54 μm^2/min, respectively. ESCs with βKO or CNQX inhibition have a similar rate of Wnt3a-bead movement to that of the WT control (**Fig. 3E**).

Altogether, our results show that WT ESCs recruit and retain Wnt3a-beads, where they are positioned further from the periphery of the cell, with limited movement. However, WT ESCs do not recruit iWnt3a-beads efficiently and have unstable interactions. ESCs position iWnt3a-beads in the periphery of the cell, where they also have more movement, and cell-bead contact is lost after a shorter on average interaction. Perturbation of the pathway components, or iGluR activity, results in impaired ability to position Wnt3a-beads close to the centre of the cell. Furthermore, while Lrp6, β-catenin and iGluR activity are required for the efficient recruitment of Wnt3a-beads, Lrp5 is important for retention and maintenance of the Wnt3a-bead contact.

We analysed the dynamics of Wnt3a-bead on the ESC membrane, and what role the pathway components have during this interaction. It is known that a Wnt3a-bead promotes orientated asymmetric cell division (ACD) in mouse ESCs (Habib et al., 2013). In order to follow the effect of bead dynamics through the process of cellular division, we studied the orientation of the spindle during mitosis.

Wnt/β-catenin pathway and iGluR activity regulate the orientation of the mitotic spindle

Wnt-mediated spindle orientation is known as an important factor in the process of ACD in several biological systems (Bertrand, 2016; Goldstein et al., 2006; Huang and Niehrs, 2014; Kaur et al., 2020; Sugioka et al., 2011; Walston et al., 2004). Spindle orientation is established and can be determined as early as the anaphase (Kiyomitsu and Cheeseman, 2013). Our high temporal resolution of live imaging every one minute allows accurate measurement at this time point. Anaphase can be clearly identified in brightfield by elongation of the cell along the axis of mitosis and separation of chromosomes (**Fig. 4A**). Precise measurement of the direction of Wnt3a signal is achieved by direct visualization of the Wnt3a-bead. The angle between the bead, the centre of the dividing cell, and the minor axis was measured (**Fig. 4B**, α). In this way, 90 degrees represents the spindle aligned directly towards the Wnt3a-bead. 0 degrees represents the spindle aligned orthogonal to the bead, a misoriented division (**Fig. 4B**).

WT ESCs divide predominantly oriented towards the Wnt3a-bead, with a most common angle of 85-90 degrees (**Fig. 4C**). This biased distribution is significantly different ($p < 0.05$) to a randomized distribution by Chi-square statistical analysis (**Fig. 4I**). This analysis compares the experimental distribution of division angles to a randomized distribution of spindle orientations. The randomized distribution (in which the Wnt-bead contact is not having an effect) assumes a non-biased accumulation of division counts at 0º-30º, 30º-60º and 60º-90º as 1/3:1/3:1/3 of the total divisions. Indeed, when presented with iWnt3a-beads, the bias towards the bead is not seen, producing a randomized distribution. An increased proportion of cells has iWnt3a-beads between 0 and 5 degrees (**Fig. 4C and I**).

Single ESCs that lack Lrp5, β-catenin, or iGluR activity, and divide with Wnt3a-beads, result in a similarly randomized distribution ($p > 0.05$, Chi-square analysis), indicating a loss of Wnt-mediated spindle orientation (**Fig. 4D, G-I**). In ESCs lacking Lrp6 (Lrp6KO and Lrp5/6dKO) division contacting a Wnt3a-bead results in a misaligned orientation. Here, the distribution is significantly different from randomized distribution ($p < 0.05$, Chi-Square statistical analysis, **Fig. 4I**). However, the experimental angle distributions of Lrp6KO and Lrp5/6dKO are significantly different to the one measured in WT ESCs dividing with a Wnt3a-bead. This is measured by two-sample Kolmogorov-Smirnov (K-S) statistical analysis, which identifies whether two data samples arise from the same distribution (assuming non-normality). In Lrp6KO, divisions are oriented mostly between 0 and 40 degrees, and in Lrp5/6dKO, the divisions are mostly between 0 and 30 degrees (**Fig. 4E-F**). While they retain some capability to align the spindle beyond a randomized orientation, neither represent efficient Wnt3a-orientated divisions. By K-S statistical analysis, all conditions, whether by inactive iWnt3a-beads, component KO, or CNQX inhibition, are

significantly different from the Wnt3a-orientated spindle seen in WT ESCs with Wnt3a-beads (**Fig. 4I**).

Disruption of the Wnt co-receptors, the downstream component β-catenin, and iGluR activity impairs the orientation of the spindle towards a source of localized Wnt3a during division. While localized Wnt3a controls spindle orientation, it also controls cell fate, producing a self-renewed Wnt3a-proximal ESC and a Wnt3a-distal prone cell to differentiation. Next we studied if the Wnt3a-spindle orientation is coupled to the cell fate determination.

iGluR activity is required for asymmetric division of pluripotency markers, while Lrp5 is dispensable

Asymmetric cell division (ACD) is the partitioning or enrichment of cellular components in one of the two daughter cells deriving from mitosis that leads to differences in the cell fate of daughter cells. We studied the role of Wnt co-receptors and β-catenin as well iGluR activity in this process.

To that end, we quantified the distribution of the pluripotency markers in post-division pairs of daughter cells in contact with Wnt3a-beads. Wnt3a-beads induces ACD in single ESCs (Habib et al., 2013). Expression of pluripotency markers allows comparison of the cell fate of the daughter cells. A higher pluripotency marker expression indicates maintenance of a naïve ESC, whereas a lower expression indicates a shift towards a more differentiated state. We seeded single cells at low density in the presence of Wnt3a-beads for 6 hours, found to be optimal for capturing cell pairs immediately after division. We then fixed, stained and analysed the divided cells, where a bead is in clear contact with only one of the two daughter cells, ensuring that cell pairs with an asymmetric presentation of the Wnt3a signal are analysed.

Cell pairs were categorized based on the distribution of pluripotency markers Rex1 and Nanog (**Fig. 5A and B**). If the cell in contact with the bead (Wnt3a-proximal) contains higher pluripotency marker signal, this indicates that the cell nearest the bead has self-renewed. Correspondingly, the Wnt3a-distal cell expresses significantly less pluripotency marker. This is named a ‘Proximal’ distribution. The corollary, where the farthest cell expresses more pluripotency marker is named a ‘Distal’ distribution. An even distribution, with no significant bias to either cell is named ‘Distributed’. Only the proximal condition represents a Wnt-orientated asymmetric cell division.

When presented with Wnt3a-beads, a large proportion of wild type ESC doublets are proximally distributed, and have therefore undergone Wnt-oriented ACD (**Fig. 5C and D**). Lrp5 KO ESCs lose the ability to align the spindle towards a Wnt3a signal (**Fig. 4D**).

However, in Lrp5 KO ESCs that have achieved a Wnt3a-oriented division and solely one cell maintains contact with the Wnt3a-bead, they retain the capability for Wnt3a-oriented ACD (**Fig. 5C-F**). This Wnt3a-oriented ACD is no longer favoured during CNQX inhibition. While a total of ~60% of cell doublets have undergone ACD when treated with CNQX, only ~30% of total doublets have a pluripotency marker distribution proximal to the localized Wnt3a (**Fig. 5C-F**).

ESCs lacking Lrp6 or β-catenin (Lrp6KO, Lrp5/6dKO, βKO) results in an impairment of ACD in any orientation (Proximal or Distal). This suggests that these cells are unable to compartmentalize protein constituents. The majority (49.11% to 76.16%) of these cell pairs have equal pluripotency marker expression in both daughter cells. This is observed in the expression of both Rex1 and Nanog (**Fig. 5C-F**).

In summary, in ESCs Lrp5 has a role in the maintenance of contact with a localized Wnt3a source, and spindle orientation towards the Wnt3a signal. In the few Lrp5KO ESCs that do divide towards a Wnt3a-bead, Wnt3a-oriented ACD is achieved with similar efficiency to WT. Both Lrp5 and Lrp6 are involved in the stabilization of the position of Wnt3a-cell contact. Lrp6, however, plays a larger role in forming the asymmetric distribution of protein components at division, alongside β-catenin. Lrp6KO in ESCs results in severely impaired activation of the Wnt/β-catenin pathway, as well as impaired recruitment and stabilisation of interaction with Wnt3a-beads. Prior to ACD, β-catenin also has roles in Wnt3a recruitment and orientation of the spindle. iGluR activity functions parallel those of Lrp6 in terms of Wnt3a recruitment and the breaking of cellular symmetry.

We have elucidated the processes and dynamics that link initial signal interaction to the asymmetric cell division that determines differences in cell fate within a pair of daughter cells. We have determined that co-receptors of the Wnt/β-catenin pathway have differing roles during interaction with a localized source of Wnt3a on the cell membrane. Furthermore, we show that iGluR activity remains coupled to components of the Wnt/β-catenin pathway in the downstream effects of spindle orientation and ACD. This suggests that crosstalk between AMPA/Kainate receptor signalling and Lrp6 activation is not only involved in signal recognition and response, as previously shown, but is coupled throughout the spatial organisation and specification of dividing ESCs by Wnt3a.

DISCUSSION

Cell fate and spatial positioning occur in concert to achieve proper tissue organization. This process is often controlled by extrinsic cues such as Wnt signals. Wnt reception has been previously shown to induce cell polarization and asymmetric cell division (ACD), in an evolutionarily conserved manner (Goldstein et al., 2006; Huang and Niehrs, 2014; Mizumoto and Sawa, 2007; Ouspenskaia et al., 2016; Sugioka et al., 2011; Walston et al., 2004). Wnt signalling plays a crucial role in the stem cell niche, where stem cells receive Wnts as a cue for self-renewal and cell fate determination (Clevers et al., 2014; Garcin and Habib, 2017). Although *in vivo* lineage tracing, genetic analysis and *in vitro* studies have provided crucial understanding of the effects of Wnt on stem cell biology (Mills et al., 2017), technical limitations have impeded the study of dynamic, localized Wnt reception at the single stem cell level. Understanding these early processes of ligand recruitment to the stem cell membrane may prove beneficial for regenerative medicine and the targeting of Wnt-related diseases. By harnessing the dynamics of Wnt ligand-cell interactions, interventions focused on Wnt ligands, receptors or other signalling components on the membrane may be made more selective, targeted, and better positioned for clinically viable strategies.

We have developed a system for the presentation of biologically active Wnt ligands covalently immobilized to a bead (Wnt-bead) (Habib et al., 2013; Lowndes et al., 2017), allowing the direct visualization of Wnt ligands during dynamic ligand-membrane interactions. Recently, we found that ESCs generate specialized cytonemes that selectively recruit self-renewal Wnt-beads in a process that requires iGluR activity (Junyent et al., 2020). Subsequently, Wnt-beads induce oriented ACD in single ESCs (Habib et al., 2013). In this manuscript, we present a temporal analysis spanning the entire duration of the stem cell—Wnt-bead interaction: from cell morpho-motility prior to contact and initial bead recruitment through cytonemes, to dynamics during Wnt-cell membrane interaction leading to the later cellular effects on spindle orientation and ACD. Initially, we revealed differences in the pattern of cytoneme formation at the population level. ESCs under CNQX inhibition, or KO for Lrp6 or β-catenin, form cytonemes at the same rate as WT ESCs. They have a mostly linear increase in the proportion of cells with cytonemes over time, reaching approximately 40% within 4 hours of attachment.

The Wnt co-receptors Lrp5 and Lrp6 have mostly been studied in the context of β-catenin dependent signalling, where they are attributed to have broadly overlapping functions (He et al., 2004; Houston and Wylie, 2002; Kelly et al., 2004; Tamai et al., 2000; Wehrli et al., 2000), albeit to different levels of efficiency (Holmen et al., 2002; MacDonald et al., 2011). Our unique system demonstrates differing roles between Lrp5 and Lrp6. The endogenous

expression of Lrp6 alone in ESCs (in Lrp5KO) results in an increased rate of cytoneme formation over WT ESCs, reaching 55.53% of cells with cytonemes after 3 hours. Together with a reduction in the rate of cytoneme formation in Lrp5/6dKO, this suggests that Lrp6 has a distinct role in the regulation of the cytoskeleton. Both Lrp5 and Lrp6 contain proline rich motifs (XPPPP) in the cytoplasmic domain that can bind to regulators of actin filaments responsible for changes to their elongation and dynamics (Brown et al., 1998; Krause et al., 2003; Lian et al., 2016; Zhu et al., 2012). Lrp6 binds Filamin A (FlnA), an anchor of transmembrane proteins to, and regulator of, the actin cytoskeleton (Lian et al., 2016). Despite 69% sequence identity overall between Lrp5 and Lrp6 (MacDonald et al., 2011), the corresponding region in Lrp5 has 37% identity. Such differences might contribute to differential roles in the organization of the actin cytoskeleton, and interaction with the machinery required for cytoneme formation/elongation. We suggest that Lrp5 may be acting in competition with Lrp6 for the interaction of Wnt-pathway components or cytoskeletal regulators. Hence, upon Lrp5 KO, this competition may be lifted, resulting in improved Lrp6-cytoskeleton interaction and the increased rate of cytoneme formation and initial Wnt3a-bead recruitment observed in Lrp5KO ESCs.

The rate of Wnt-bead accumulation by KO cells is also affected. During the early interaction, WT ESCs use cytonemes to recruit and retain Wnt3a-beads efficiently, reaching 66.75% of cells with beads after 12 hours, positioning them near the centre of the cell with limited movement. WT ESCs are unable to recruit iWnt3a-beads with the same efficiency: ESCs maintain iWnt3a-beads nearer the periphery of the cell, and their interactions are shorter and less stable. KO of pathway components Lrp5, Lrp6 or β-catenin, or inhibition of iGluRs, also reduces the ability to position a Wnt3a-bead on the membrane near the centre of the cell. While Lrp6, β-catenin and iGluR activity play an important role in the recruitment of Wnt3a-beads, Lrp5 is important for the stabilization of the Wnt-cell interaction both in space and over time.

The control of positioning of the Wnt3a-bead in WT ESCs may facilitate efficient protein interactions required for signal transduction, enhancing downstream pathway activation. Beyond the ligand-receptor binding, Wnt-pathway component polarization (Capelluto et al., 2002) and oligomerization (Cong et al., 2004) are suggested to play roles in the enhancement or modulation of Wnt signaling (Bilic et al., 2007). Here, the spatial stabilization and colocalization of upstream and downstream pathway components at a 'signalling hub' may be critical for efficient signal transmission. Membrane receptors, including glutamate receptors (Yang et al., 2006), have been demonstrated to flow from membrane protrusion towards the centre of the cell. This motion can be promoted by directed movement of the actin cytoskeleton (Hanley, 2014; Yu et al., 2010) and its efficiency

can be governed by the activation of the pathway (Hartman et al., 2009). Areas of relative membrane concavity, such as the cell centre away from the periphery, have also been shown to enhance membrane receptor interactions with intracellular components (Rangamani et al., 2013). This process may be required for the enhancement, or maximization, of signalling transmission (Schmick and Bastiaens, 2014).

Following early Wnt-bead recruitment and upon progression to mitosis, WT ESCs orientate the spindle towards the source of localized Wnt3a at anaphase. Perturbation of the Wnt/β-catenin pathway components or iGluR activity inhibition resulted in significant impairment of the alignment of the spindle to localized Wnt3a. Furthermore, an asymmetric presentation of Wnt3a at division leads to the asymmetric distribution of pluripotency markers in the dividing WT ESCs. The Wnt-proximal cell retains the majority of pluripotency marker expression in these doublets, indicating self-renewal, while the Wnt-distal cell has a more differentiated fate. Asymmetric cell division is impaired when the ESCs lack Lrp6, β-catenin or iGluR activity. Lrp5 KO ESCs remain able to asymmetrically segregate pluripotency markers to the proximal cell. This data suggests a differential requirement for Lrp6 and Lrp5 in ACD, which is also β-catenin dependent, as corroborated by severe impairment of ACD in βKO.

Our study also distinguishes β-catenin dependent and independent processes in early Wnt ligand-receptor interaction and cellular outcomes. Wnt-recruitment, Wnt-positioning, spindle orientation, and ACD, while requiring the activity of Wnt co-receptors and iGluRs, are β-catenin dependent. The rate of cytoneme formation, cell motility, and localized Wnt-retention, however, appear to be β-catenin independent, despite involvement of Wnt co-receptors Lrp5/6. We previously found that β-catenin had an inverse relationship with the number of cytonemes in ESCs (Junyent et al., 2020). Furthermore, while individual interactions of cytoneme and Wnt3a-bead were equally efficient in WT and βKO ESCs (Junyent et al., 2020), here we demonstrate that the population-level accumulation of Wnt3a-beads is severely attenuated. Our results in the β-catenin and co-receptor KOs blur the lines between canonical and non-canonical Wnt pathways, instead suggesting an integrated, complex response to localized Wnt reception that affects stem cell biology in multiple aspects.

iGluR activity, and its crosstalk with the Wnt/β-catenin pathway, controls recruitment of Wnt signals in ESCs. Surprisingly, we found that iGluR activity is further involved in many of the subsequent processes of Wnt-interaction. At the population level, iGluR inhibition reduces the accumulation of Wnt3a-bead, despite having no significant effect on the rate cytoneme formation or cell motility. iGluR activity is shown to have a major role in the dynamics of Wnt on the membrane, spindle orientation, and to an extent, the Wnt3a-mediated determination

of cell fate. We propose that crosstalk between the activity of iGluRs and Lrp6 controls the prolonged coupling of the two pathways, resulting in highly overlapping effects of Lrp6 or iGluR perturbation.

As many stem cells express glutamatergic receptors (Skerry and Genever, 2001) and rely on Wnts for their self-renewal (Clevers et al., 2014), investigation of equivalent effects in the biology of adult stem cells is required. Our results suggest a crosstalk between iGluRs and Wnt-pathway activity in ESCs that affects cell and signal kinetics throughout Wnt signal recruitment and the cellular outcome of oriented ACD. The iGluR-Wnt pathway crosstalk may therefore prove to be a pervasive mechanism in the coordination throughout cell fate determination and tissue patterning in many cell types and biological systems.

MATERIALS AND METHODS

Cell culture

Wild-type W4 (129S6/SvEvTac) mouse ESCs or ESCs knock-out for Lrp5, Lrp6 or Lrp5/6dKO (Junyent et al., 2020) were maintained in ESC basal media containing Advanced DMEM/F12 (cat. num. 12634028, Life Technologies), 10% ESC-qualified fetal bovine serum (eFBS, cat. num. ES-009-B, Millipore), 1% penicillin-streptomycin (P-S, cat. num. P4333, Sigma), 2 mM Glutamax (cat. num. 35050061, Life Technologies), 50 µM β-mercaptoethanol (2ME, cat. num. 21985-023, Gibco) and 1000 U/mL recombinant Leukemia Inhibitory Factor (LIF; cat. num. 130-095-775, Milteny), supplemented with with 2i: MEK inhibitor PD0325901 (1 µM, cat. num. 130-104-170, Miltenyi) and GSK3 inhibitor CHIR99021 (3 µM, cat. num. 130-104-172, Miltenyi). Heterozygous β-catenin deficient ($\beta^{f/-}$) ESCs, with an inducible floxed β-catenin allele, and stably carrying a Cre-ER-T2 cassette under the control of a chicken β-actin promoter (Raggioli et al., 2014) were cultured in the same conditions. Media was changed daily, and cells were grown at low density until formation of mid-sized colonies before passaging (every 3-4 days). To passage ESCs, colonies were rinsed with PBS, trypsinised, neutralized and centrifuged at 1.2 x *g* for 4 minutes. Pelleted cells were resuspended in ESC basal media and counted to obtain 7,000 cells/well and transferred to a clean tissue culture-treated 6-well plate. In some experiments, 24 hours prior to use, 2i was withdrawn and replaced with soluble Wnt3a protein (200 ng/mL).

Generation of inducible β-catenin knock-out from $\beta^{f/-}$ cells was achieved through the addition of 0.1 µg/mL 4-hydroxy-tamoxifen (4-HT) (cat. num. H6278, Sigma) to the media every 24 hours for 72 hours (referred as βKO in the text). βKO cells were always 4-HT treated for 3 days before experimentation.

All cell lines were maintained at 37ºC, 5%CO_2 and were routinely tested for mycoplasma infection.

Preparation of Wnt3a-microbeads

Recombinant Wnt3a proteins were produced as described before (Habib et al., 2013; Junyent et al., 2020), or purchased (cat. num. 1324-WN, R&D systems). Wnt3a proteins were immobilized to 2.8 µm carboxilyc acid coated Dynabeads® (cat. num. 14305D, ThermoFisher), as described before (Habib et al., 2013; Junyent et al., 2020; Lowndes et al., 2017). Briefly, the carboxylic acid groups on the Dynabeads® were activated by 30-minute incubation with carbodiimide (cat. num. E7750-1G, Sigma) and N-hydroxyl succinamide (cat. num. 56480-25G, Sigma) (50 mg/mL each, dissolved in 25 mM cold 2-(N-morpholino) ethanesulfonic acid (MES) (cat. num. M3671-50G, Sigma) buffer (pH5) with constant

rotation. Following activation, beads were retained by using a magnet and washed three times with 25 mM MES buffer (pH5). Soluble Wnt3a protein (500 ng) was diluted 1:5 in MES buffer (pH5) and incubated with the beads for 1 hour with constant agitation, at room temperature (RT). Beads were washed again three times with PBS (pH 7.4) before storage in media containing 10% FBS at 4°C. Inactivation of Wnt3a beads was achieved through incubation with 10 mM Dithiothreitol (DTT; Life Technologies, #P2325) for 30 minutes at 37°C. Following incubation with DTT, beads were washed three times in PBS before storage in media containing 10% FBS at 4°C (up to 10 days). Bead activity was validated as described before (Habib et al., 2013; Junyent et al., 2020; Lowndes et al., 2017)

Live-cell imaging and image analysis and spindle orientation

ESCs were seeded at 2,500 cells per well of a clear-bottomed, tissue culture treated, plastic, black 96 well plate in complete media containing LIF (no 2i). 0.3 µg Wnt3a-beads were added per well. The 96 well plate was placed into the Zeiss inverted Axio Imager epifluorescence microscope, equipped with a CoolSNAP HQ2 CCD camera. Cells were allowed to settle in the microscope at 37°C, 5% CO_2 for 30 minutes prior to imaging. Between 20-30 positions were selected, and cells were imaged at 10X (N/A = 0.3) in brightfield every 1 minute for 12-15 hours.

The resulting videos were analysed to measure the percentage of cells with cytonemes, the percentage of cells with beads and the bead retention time in all conditions. “Manual tracking” tool in Fiji (ImageJ) was used to measure the Wnt-bead position, the cell-centre position and the radius of the cell every minute for 180 minutes (3h) after bead recruitment through a cytoneme. The resulting data was used to measure cell movement, position of the Wnt bead on top of the cell and Wnt bead movement, normalized to cell movement.

Cells dividing in contact with a Wnt3a-bead were measured to analyse spindle orientation. The “Angle” tool in Fiji (ImageJ) was used to measure the angle between the minor axis and the Wnt-bead position at the same point in anaphase for all conditions (**Fig. 4A and B**).

Immunofluorescence and measurement of asymmetric cell division

ESCs were seeded at 3,000 cells/well + 0.3 µg Wnt3a-bead/well onto human fibronectin (10 µg/mL, cat. um. 7340101, VWR/SLS) coated 8-well slides (cat. num. 80828, Thistle Scientific) in complete media containing LIF (no 2i). Slides were incubated for 7h at 37°C, 5%CO_2. After incubation, media was pipetted out and cells were fixed with 4%PFA for 8 min at room temperature (RT). Cells were then washed 3 times in staining buffer (Phosphate buffered saline (PBS, cat. num. d8537, Sigma), with 0.1% Bovine Serum Albumin (cat. num. A8806, Sigma), 0.05% Sodium Azide and 0.001% Tween20 (cat. num. P2287, Sigma)) for 5

minutes each. Slides were incubated in primary antibody diluted in staining buffer at 4°C overnight. Primary antibodies used were anti-Rex1 (Rabbit; Abcam, ab28141), anti-Nanog (Rabbit, Reprocell, RCAB002P-F) and anti-β-catenin (Mouse; BD Transduction, #610154). Then, slides were carefully washed 3 times for 5 minutes in staining buffer and incubated with AlexaFluor-conjugated secondary antibodies (Life Technologies) diluted in staining buffer, for 1h at RT. Final washes were performed with staining buffer containing Hoecht 33342 (cat. num. H3570, Life Technologies) at 1:2000 dilution. Slides were carefully mounted with ProLong mounting media (cat. num. P10144, Life Technologies) and curated for 24-48h before imaging. Slides were imaged on a Zeiss inverted Axio Imager epifluorescence microscope using Zen 2 (Blue edition) software, 40x (NA = 1.3), equipped with a CoolSNAP HQ2 CCD camera. Z-stacks were taken according to the optimal interval, and the range obtained based on β-catenin signal. Images were processed, deconvolved, and quantified by supervised quantification using Volocity software (Perkin Elmer).

Supervised quantification involved reconstructing the cell using fluorescence staining and manual identification of divided cells. The cell proximal to the bead was defined as the region of interest (ROI), and the distal cell was defined as the fluorescence minus the proximal cell (ROI). Cells were compartmentalized based on DAPI staining for nucleus and the remainder of the cell minus DAPI comprised the cytoplasmic region. Protein distribution in the doublets was established as follow: Proximal, >55% of protein in bead-proximal cell; Distributed, 55% to 45% of protein in bead-proximal cell; Distal, <45% of protein in bead-proximal cell.

Live cell holotomographic microscopy

Holotomographic images were obtained by using 3D Cell Explorer (Nanolive) microscope equipped with a 60x (N.A. 0.8) lens. Images were analysed using STEVE® software (Nanolive) and Fiji (ImageJ).

Fluorescence Activated Cell Sorting

Fluorescence activated cell sorting (FACS) was employed to detect Wnt3a response of WT or KO ESCs stably infected with 7xTCF-eGFP//SV40-mCherry (Junyent et al., 2020). Infected cells were sorted to gain a pure mCherry+ population. Following stimulation with Wnt3a or control media (ESC basal media) for 24h, cells were harvested using 0.25% trypsin-EDTA solution, filtered and analyzed using the FACSFortessa system (BD Biosciences). The gating strategy included gating for SSC-FSC, SSC-A-SSC-W, SSC-DAPI (alive cells), SSC-PE Texas Red (mCherry+ cells), and SSC-FITC (eGFP+ cells). Cells were prepared for FACS and analysis was performed as described before. Analysis was performed using FlowJo software (FlowJo).

Statistical analysis

Data representation and statistical analysis were performed using Prism (GraphPad), as described in the figures. ANOVA (one- or two-way) analysis, followed by Tukey's multiple comparisons test was performed to compare data between conditions. For analysis of spindle orientation, the Kolmogorov-Smirnov statistical test was performed to compare between conditions of non-normally distributed data and Chi-square analysis was performed to compare between observed data and the expected/randomized distribution. The statistical analysis used for each assay is described in the figure legends. In all experiments, biological replicates (n) for each assay comprise of experiments performed independently from one another, and as such are from different cultured populations/passages of cells, different sessions of imaging/measurement, and independent media/reagent/cell dilution. Sample sizes (N) were selected such that the power of the statistical analysis performed was sufficient, in accordance with previous studies (Habib et al., 2013; Junyent et al., 2020). Outliers were considered as individual data points significantly outside the range of possible/meaningful values for each assay and were excluded from subsequent analysis. For all figures, symbols indicate statistical significance as follows: $*p < 0.05$, $**p < 0.01$, $***p< 0.001$, $****p< 0.0001$. Non-significance was set as $p > 0.05$. All numerical source data, as well as statistical analysis results including 95% confidence interval and adjusted *p*-values can be consulted in the source data file for each figure.

ACKNOWLEDGEMENTS

We acknowledge financial support from the Department of Health via the National Institute for Health Research (NIHR) Comprehensive Biomedical Research Centre award to the Guy's & St Thomas National Health Service Foundation Trust in partnership with King's College London and the King's College Hospital NHS Foundation Trust. This work was supported by a Sir Henry Dale Fellowship (102513/Z/13/Z) to S.J.H.

CONTRIBUTION

S.J., J.R. and S.J.H. designed the study, performed experiments and analysed data, wrote the manuscript and prepared figures. J.L.A.S, C.L.G and T-J.T. performed experiments and analysed data. M.W. analysed data. S.J.H lead the project and provided financial support for the project.

COMPETING INTERESTS

No competing interests.

REFERENCES

Akong K, McCartney BM, Peifer M. 2002. Drosophila APC2 and APC1 have overlapping roles in the larval brain despite their distinct intracellular localizations. *Dev Biol* **250**:71–90. doi:10.1006/dbio.2002.0777

Bahmanyar S, Kaplan DD, DeLuca JG, Giddings TH, O'Toole ET, Winey M, Salmon ED, Casey PJ, Nelson WJ, Barth AIM. 2008. β-catenin is a Nek2 substrate involved in centrosome separation. *Genes Dev* **22**:91–105. doi:10.1101/gad.1596308

Bertrand V. 2016. B-Catenin-Driven Binary Cell Fate Decisions in Animal Development. *Wiley Interdiscip Rev Dev Biol* **5**:377–388. doi:10.1002/wdev.228

Bienz. 2005. β-Catenin: A Pivot between Cell Adhesion and Wnt Signalling Mutual. *Curr Biol* **15**:64–67. doi:10.1016/j.cub.2004.12.058

Bilic J, Huang Y-L, Davidson G, Zimmermann T, Cruciat C-M, Bienz M, Niehrs C. 2007. Wnt Induces LRP6 Signalosomes and Promotes Dishevelled-Dependent LRP6 Phosphorylation. *Science (80-)* **316**:1619–1622. doi:10.1126/science.1137065

1 Brown SD, Twells RCJ, Hey PJ, Cox RD, Levy ER, Soderman AR, Metzker ML, Caskey CT,
2 Todd JA, Hess JF. 1998. Isolation and characterization of LRP6, a novel member of the
3 low density lipoprotein receptor gene family. *Biochem Biophys Res Commun* **248**:879–
4 888. doi:10.1006/bbrc.1998.9061

5 Capelluto DGS, Kutateladze TG, Habas R, Finkielstein C V., He X, Overduin M. 2002. The
6 DIX domain targets dishevelled to actin stress fibres and vesicular membranes. *Nature*
7 **419**:726–729. doi:10.1038/nature01056

8 Clevers H. 2006. Wnt/β-Catenin Signaling in Development and Disease. *Cell* **127**:469–480.
9 doi:10.1016/j.cell.2006.10.018

10 Clevers H, Loh KM, Nusse R. 2014. Stem cell signaling. An integral program for tissue
11 renewal and regeneration: Wnt signaling and stem cell control. *Science* **346**:1248012.
12 doi:10.1126/science.1248012

13 Cong F, Schweizer L, Varmus H. 2004. Wnt signals across the plasma membrane to
14 activate the β-catenin pathway by forming oligomers containing its receptors, Frizzled
15 and LRP. *Development* **131**:5103–5115. doi:10.1242/dev.01318

16 Davidson G, Shen J, Huang YL, Su Y, Karaulanov E, Bartscherer K, Hassler C, Stannek P,
17 Boutros M, Niehrs C. 2009. Cell Cycle Control of Wnt Receptor Activation. *Dev Cell*
18 **17**:788–799. doi:10.1016/j.devcel.2009.11.006

19 Fuerer C, Nusse R. 2010. Lentiviral vectors to probe and manipulate the Wnt signaling
20 pathway. *PLoS One* **5**. doi:10.1371/journal.pone.0009370

21 Garcin CL, Habib SJ. 2017. A Comparative Perspective on Wnt / β -Catenin Signalling in
22 Cell Fate Determination In: J.-P. Tassan JZK, editor. Asymmetric Cell Division in
23 Development, Differentiation and Cancer, Results and Problems in Cell Differentiation
24 61, DOI 10.1007/978-3-319-53150-2_15. Springer International Publishing AG. pp.
25 323–350. doi:10.1007/978-3-319-53150-2

26 Goldstein B, Takeshita H, Mizumoto K, Sawa H. 2006. Wnt signals can function as positional
27 cues in establishing cell polarity. *Dev Cell* **10**:391–6. doi:10.1016/j.devcel.2005.12.016

28 Habib SJ, Chen B-C, Tsai F-C, Anastassiadis K, Meyer T, Betzig E, Nusse R. 2013. A
29 Localized Wnt Signal Orients Asymmetric Stem Cell Division in Vitro. *Science (80-)*
30 **339**:1445–1448. doi:10.1126/science.1231077

31 Hanley JG. 2014. Actin-dependent mechanisms in AMPA receptor trafficking. *Front Cell*
32 *Neurosci* **8**:1–8. doi:10.3389/fncel.2014.00381

Hartman NC, Nye JA, Groves JT. 2009. Cluster size regulates protein sorting in the immunological synapse. *Proc Natl Acad Sci U S A* **106**:12729–12734. doi:10.1073/pnas.0902621106

He X, Semenov M, Tamai K, Zeng X. 2004. LDL receptor-related proteins 5 and 6 in Wnt/β-catenin signaling: Arrows point the way. *Development* **131**:1663–1677. doi:10.1242/dev.01117

Hendriksen J, Jansen M, Brown CM, van der Velde H, van Ham M, Galjart N, Offerhaus GJ, Fagotto F, Fornerod M. 2008. Plasma membrane recruitment of dephosphorylated β-catenin upon activation of the Wnt pathway. *J Cell Sci* **121**:1793–1802. doi:10.1242/jcs.025536

Holmen SL, Salic A, Zylstra CR, Kirschner MW, Williams BO. 2002. A novel set of Wnt-Frizzled fusion proteins identifies receptor components that activate β-catenin-dependent signaling. *J Biol Chem* **277**:34727–34735. doi:10.1074/jbc.M204989200

Houston DW, Wylie C. 2002. Cloning and expression of Xenopus Lrp5 and Lrp6 genes. *Mech Dev* **117**:337–342. doi:10.1016/S0925-4773(02)00205-8

Huang P, Senga T, Hamaguchi M. 2007. A novel role of phospho-β-catenin in microtubule regrowth at centrosome. *Oncogene* **26**:4357–4371. doi:10.1038/sj.onc.1210217

Huang YL, Niehrs C. 2014. Polarized Wnt signaling regulates ectodermal cell fate in Xenopus. *Dev Cell* **29**:250–257. doi:10.1016/j.devcel.2014.03.015

James RG, Conrad WH, Moon RT. 2008. b-Catenin-Independent Wnt Pathways: Signals, Core Proteins, and Effectors, Wnt Signaling, Volume I: Pathway Methods and Mammalian Models. doi:10.1007/978-1-59745-249-6

Junyent S, Garcin CL, Szczerkowski JLA, Trieu T-J, Reeves J, Habib SJ. 2020. Specialized cytonemes induce self-organization of stem cells. *Proc Natl Acad Sci* **117**:7236–7244. doi:10.1073/pnas.1920837117

Kaur S, Mélénec P, Murgan S, Bordet G, Recouvreux P, Lenne P-F, Bertrand V. 2020. Wnt ligands regulate the asymmetric divisions of neuronal progenitors in C. elegans embryos . *Development* dev.183186. doi:10.1242/dev.183186

Kelly OG, Pinson KI, Skarnes WC. 2004. The Wnt co-receptors Lrp5 and Lrp6 are essential for gastrulation in mice. *Development* **131**:2803–2815. doi:10.1242/dev.01137

Kikuchi K, Niikura Y, Kitagawa K, Kikuchi A. 2010. Dishevelled, a Wnt signalling component, is involved in mitotic progression in cooperation with Plk1. *EMBO J* **29**:3470–83.

doi:10.1038/emboj.2010.221

Kiyomitsu T, Cheeseman IM. 2013. XCortical dynein and asymmetric membrane elongation coordinately position the spindle in anaphase. *Cell* **154**:391. doi:10.1016/j.cell.2013.06.010

Komiya Y, Habas R. 2008. Wnt signal transduction pathways. *Organogenesis* **4**:68–75. doi:10.4161/org.4.2.5851

Krause M, Dent EW, Bear JE, Loureiro JJ, Gertler FB. 2003. Ena/VASP Proteins: Regulators of the Actin Cytoskeleton and Cell Migration. *Annu Rev Cell Dev Biol* **19**:541–564. doi:10.1146/annurev.cellbio.19.050103.103356

Langton PF, Kakugawa S, Vincent J-P. 2016. Making, Exporting, and Modulating Wnts. *Trends Cell Biol* **26**:756–765. doi:10.1016/j.tcb.2016.05.011

Lian G, Dettenhofer M, Lu J, Downing M, Chenn A, Wong T, Sheen V. 2016. Filamin A- and formin 2-dependent endocytosis regulates proliferation via the canonical wnt pathway. *Dev* **143**:4509–4520. doi:10.1242/dev.139295

Lowndes M, Junyent S, Habib SJ. 2017. Constructing cellular niche properties by localized presentation of Wnt proteins on synthetic surfaces. *Nat Protoc* **12**:1498–1512. doi:10.1038/nprot.2017.061

MacDonald BT, Semenov M V., Huang H, He X. 2011. Dissecting molecular differences between Wnt coreceptors LRP5 and LRP6. *PLoS One* **6**. doi:10.1371/journal.pone.0023537

Martello G, Smith A. 2014. The nature of embryonic stem cells. *Annu Rev Cell Dev Biol* **30**:647–675. doi:10.1146/annurev-cellbio-100913-013116

McCartney BM, Dierick HA, Kirkpatrick C, Moline MM, Baas A, Peifer M, Bejsovec A. 1999. Drosophila APC2 is a cytoskeletally-associated protein that regulates wingless signaling in the embryonic epidermis. *J Cell Biol* **146**:1303–1318. doi:10.1083/jcb.146.6.1303

Mills KM, Szczerkowski JLA, Habib SJ. 2017. Wnt ligand presentation and reception: from the stem cell niche to tissue engineering. *Open Biol* **7**:170140. doi:10.1098/rsob.170140

Mizumoto K, Sawa H. 2007. Cortical β-Catenin and APC Regulate Asymmetric Nuclear β-Catenin Localization during Asymmetric Cell Division in C. elegans. *Dev Cell* **12**:287–299. doi:10.1016/j.devcel.2007.01.004

Niehrs C, Acebron SP. 2012. Mitotic and mitogenic Wnt signalling. *EMBO J* **31**:2705–2713.

doi:10.1038/emboj.2012.124

Nusse R, Clevers H. 2017. Wnt/β-Catenin Signaling, Disease, and Emerging Therapeutic Modalities. *Cell* **169**:985–999. doi:10.1016/j.cell.2017.05.016

Ouspenskaia T, Matos I, Mertz AF, Fiore VF, Fuchs E. 2016. WNT-SHH Antagonism Specifies and Expands Stem Cells prior to Niche Formation. *Cell* **164**:156–169. doi:10.1016/j.cell.2015.11.058

Raggioli A, Junghans D, Rudloff S, Kemler R. 2014. Beta-Catenin Is Vital for the Integrity of Mouse Embryonic Stem Cells. *PLoS One* **9**:e86691. doi:10.1371/journal.pone.0086691

Rangamani P, Lipshtat A, Azeloglu EU, Calizo RC, Hu M, Ghassemi S, Hone J, Scarlata S, Neves SR, Iyengar R. 2013. XDecoding Information in Cell Shape. *Cell* **154**:1356. doi:10.1016/j.cell.2013.08.026

Rim EY, Kinney LK, Nusse R. 2020. Beta-catenin-mediated Wnt signal transduction proceeds through an endocytosis-independent mechanism. *Mol Biol Cell* mbc.E20-02-0114. doi:10.1091/mbc.E20-02-0114

Salinas PC. 2007. Modulation of the microtubule cytoskeleton: a role for a divergent canonical Wnt pathway. *Trends Cell Biol* **17**:333–342. doi:10.1016/j.tcb.2007.07.003

Schmick M, Bastiaens PIH. 2014. The interdependence of membrane shape and cellular signal processing. *Cell* **156**:1132–1138. doi:10.1016/j.cell.2014.02.007

Sedgwick AE, D'Souza-Schorey C. 2016. Wnt signaling in cell motility and invasion: Drawing parallels between development and cancer. *Cancers (Basel)* **8**:1–15. doi:10.3390/cancers8090080

Skerry TM, Genever PG. 2001. Glutamate signalling in non-neuronal tissues. *Trends Pharmacol Sci* **22**:174–181. doi:10.1016/S0165-6147(00)01642-4

Stamatakou E, Hoyos-Flight M, Salinas PC. 2015. Wnt signalling promotes actin dynamics during axon remodelling through the actin-binding protein Eps8. *PLoS One* **10**:1–19. doi:10.1371/journal.pone.0134976

Stanganello E, Zahavi EE, Burute M, Smits J, Jordens I, Maurice MM, Kapitein LC, Hoogenraad CC. 2019. Wnt Signaling Directs Neuronal Polarity and Axonal Growth. *iScience* **13**:318–327. doi:10.1016/j.isci.2019.02.029

Sugioka K, Mizumoto K, Sawa H. 2011. Wnt regulates spindle asymmetry to generate asymmetric nuclear β-catenin in C. elegans. *Cell* **146**:942–954. doi:10.1016/j.cell.2011.07.043

Tahinci E, Thorne CA, Franklin JL, Salic A, Christian KM, Lee LA, Coffey RJ, Lee E. 2007. Lrp6 is required for convergent extension during Xenopus gastrulation. *Development* **134**:4095–4106. doi:10.1242/dev.010272

Takada R, Satomi Y, Kurata T, Ueno N, Norioka S, Kondoh H, Takao T, Takada S. 2006. Monounsaturated Fatty Acid Modification of Wnt Protein: Its Role in Wnt Secretion. *Dev Cell* **11**:791–801. doi:10.1016/j.devcel.2006.10.003

Tamai K, Semenov M, Kato Y, Spokony R, Liu C, Katsuyama Y, Hess F, Saint-Jeannet JP, He X. 2000. LDL-receptor-related proteins in Wnt signal transduction. *Nature* **407**:530–535. doi:10.1038/35035117

ten Berge D, Kurek D, Blauwkamp T, Koole W, Maas A, Eroglu E, Siu RK, Nusse R. 2011. Embryonic stem cells require Wnt proteins to prevent differentiation to epiblast stem cells. *Nat Cell Biol* **13**:1070–5. doi:10.1038/ncb2314

Walston T, Tuskey C, Edgar L, Hawkins N, Ellis G, Bowerman B, Wood W, Hardin J. 2004. Multiple Wnt signaling pathways converge to orient the mitotic spindle in early C. elegans embryos. *Dev Cell* **7**:831–841. doi:10.1016/j.devcel.2004.10.008

Wehrli M, Dougan ST, Caldwell K, O'Keefe L, Schwartz S, Valzel-Ohayon D, Schejter E, Tomlinson A, DiNardo S. 2000. Arrow encodes an LDL-receptor-related protein essential for Wingless signalling. *Nature* **407**:527–530. doi:10.1038/35035110

Willert K, Brown JD, Danenberg E, Duncan AW, Weissman IL, Reya T, Yates JR, Nusse R. 2003. Wnt proteins are lipid-modified and can act as stem cell growth factors. *Nature* **423**:448–452. doi:10.1038/nature01611

Willert K, Nusse R. 2012. Wnt proteins. *Cold Spring Harb Perspect Biol* **4**:1–14. doi:10.1101/cshperspect.a007864

Yang G, Huang A, Zhu S, Xiong W. 2006. It is time to move: Role of lateral diffusion in AMPA receptor trafficking. *J Neurosci* **26**:9082–9083. doi:10.1523/JNEUROSCI.3018-06.2006

Ying Q-L, Wray J, Nichols J, Batlle-Morera L, Doble B, Woodgett J, Cohen P, Smith A. 2008. The ground state of embryonic stem cell self-renewal. *Nature* **453**:519–523. doi:10.1038/nature06968

Yu C han, Wu HJ, Kaizuka Y, Vale RD, Groves JT. 2010. Altered actin centripetal retrograde flow in physically restricted immunological synapses. *PLoS One* **5**:1–9. doi:10.1371/journal.pone.0011878

Zhu Y, Tian Y, Du J, Hu Z, Yang L, Liu J, Gu L. 2012. Dvl2-dependent activation of Daam1 and RhoA regulates Wnt5a-induced breast cancer cell migration. *PLoS One* **7**. doi:10.1371/journal.pone.0037823

FIGURES AND FIGURE LEGENDS

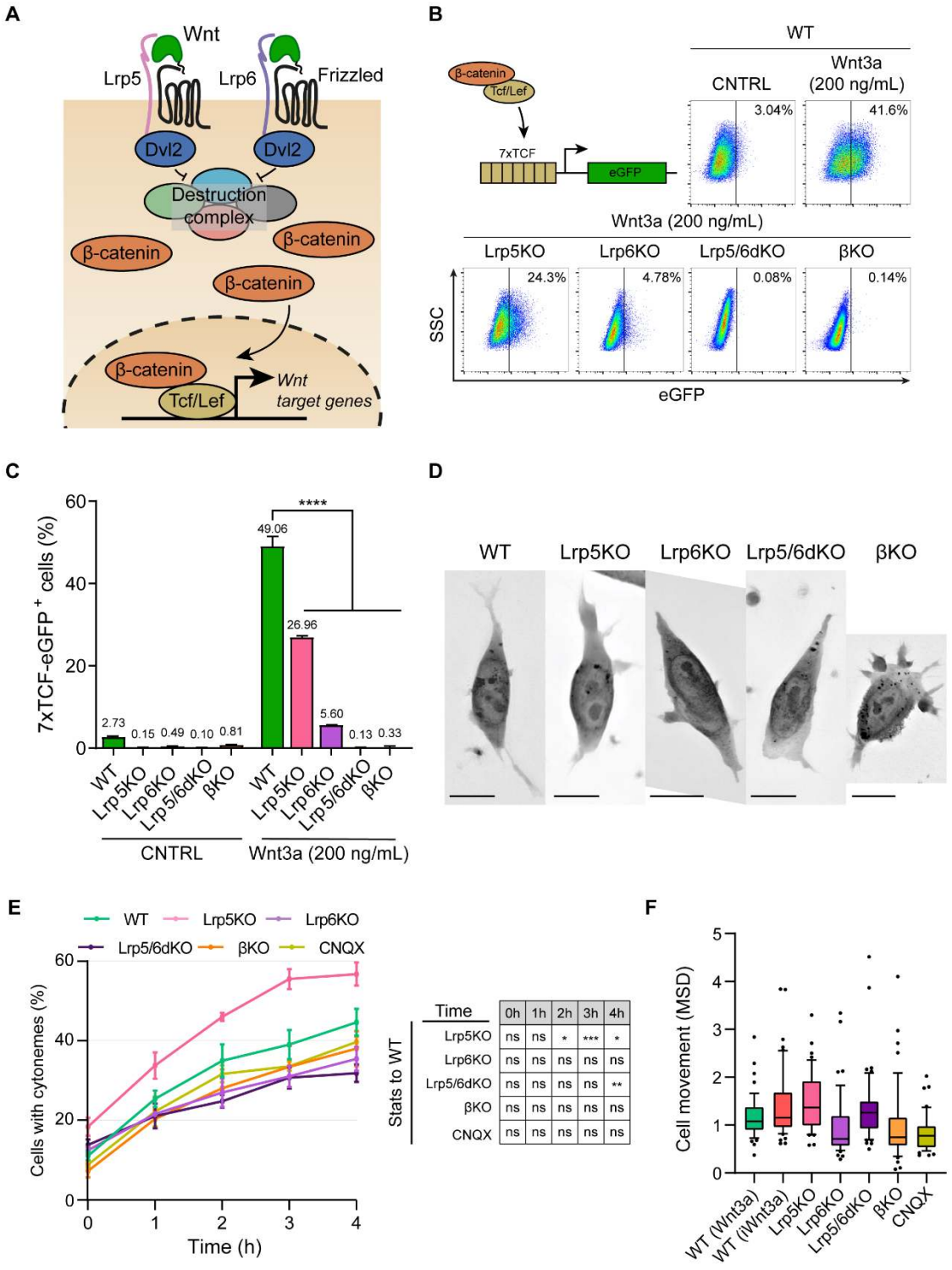

FIGURE 1. The requirements of components of the Wnt/β-catenin for Wnt responsiveness and cytoneme formation.

A. Schematic and simplified representation of the Wnt/β-catenin pathway. Wnt binding to the receptor Frizzled and the co-receptors Lrp5 and Lrp6 induces the inhibition of the β-catenin

destruction complex (Axin2, Gsk3, Ck1, APC) through Dvl2. β-catenin is stabilized and translocated to the nucleus, where it binds Tcf/Lef to initiate the transcription of Wnt target genes.

B. (*Top left*) Schematic representation of the 7xTCF-eGFP Wnt/β-catenin reporter. (*Top right* and *Bottom*) Representative dot-plots depicting the levels of eGFP expression in WT or Wnt pathway KO ESCs carrying the 7xTCF-eGFP reporter and treated with CNTRL solution or 200 ng/mL soluble Wnt3a for 24h. Y axis is SSC.

C. Quantification of the percentage of 7xTCF-eGFP^{+} cells, as described in **B**. n ≥ 3. Bar is mean, error bars indicate SEM. Stars indicate statistical significance calculated by two-way ANOVA with Tukey multiple comparison tests, as follows: ****$p < 0.0001$.

D. Representative images of the protrusions generated by WT or Wnt pathway KO ESCs, imaged by holographic-tomographic 3D microscopy. Scale bars, 20 µm.

E. Quantification of the percentage of WT ESCs, Wnt pathway KO ESCs, or WT ESCs treated with 10 µM CNQX, with cytonemes at 0 to 4 hours after seeding. Line is centred on mean, error bars indicate SEM. n ≥ 3, N ≥ 30 cells per timepoint and per n. Stars in box (*right*) indicate statistical significance to WT, calculated by two-way ANOVA with Tukey multiple comparison tests, as follows: ns (*non-significant*, $p > 0.05$) *$p < 0.05$, **$p < 0.01$, ***$p < 0.001$.

F. Quantification of cell movement, presented as mean squared displacement (MSD), for WT ESCs co-cultured with Wnt3a-beads or iWnt3a-beads, Wnt pathway KO ESCs co-cultured with Wnt3a-beads, or WT ESCs treated with 10 µM CNQX and co-cultured with Wnt3a-beads. Cells were tracked for 3h after protrusion generation. Box represents median and quartiles, error bars represent 10-90 percentile, dots are data outside 10-90 percentile range. Data is pooled from n ≥ 3 experiments, total of N ≥ 44 cells. Statistical non-significance to WT condition was verified by one-way ANOVA with Tukey multiple comparison test.

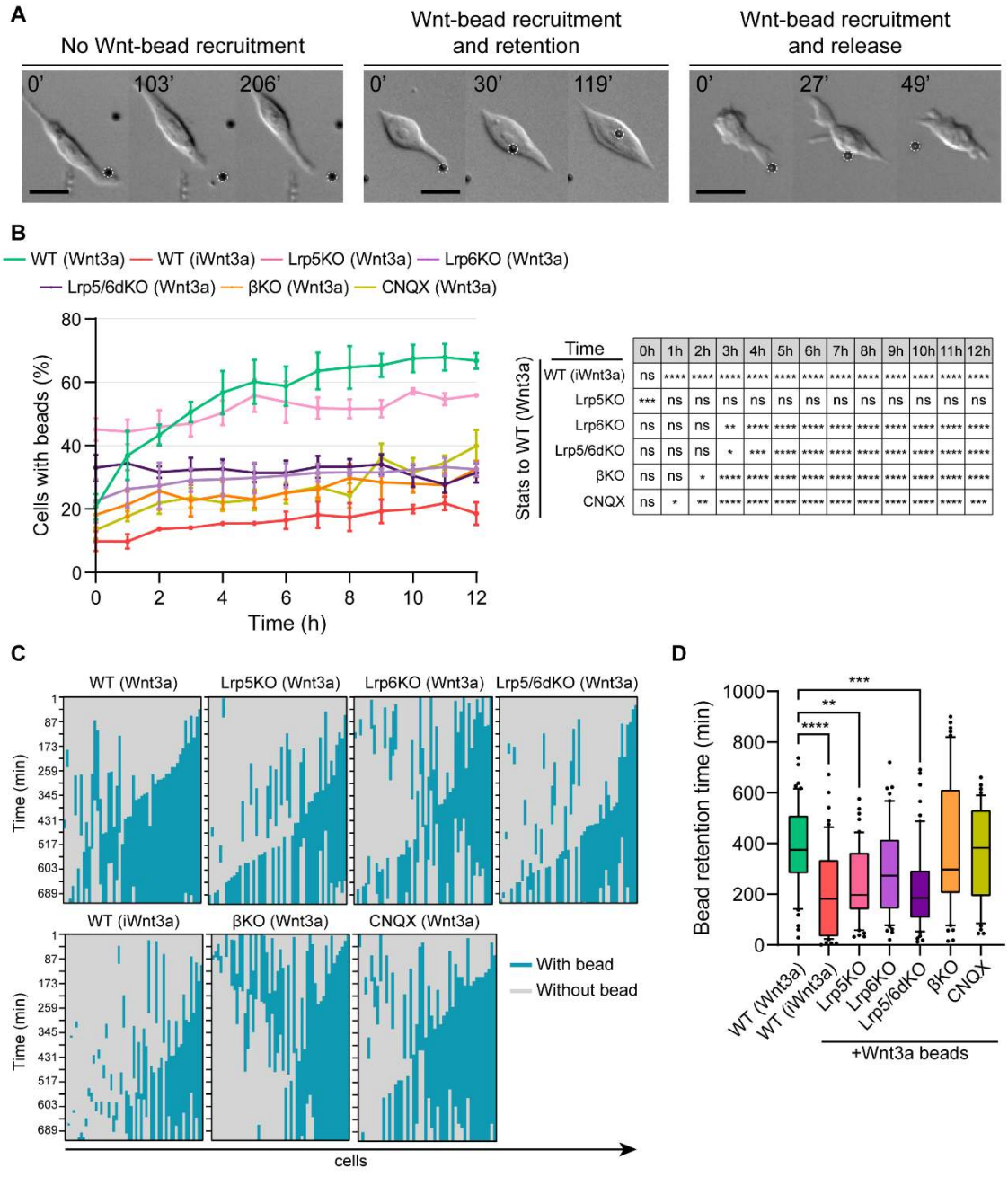

FIGURE 2. Wnt co-receptors and iGluR activity orchestrate the interaction dynamics between localized Wnt3a and the ESC membrane

A. Representative frames of time-course live imaging displaying an ESC contacting a Wnt-bead without further recruitment (*left*), an ESC contacting a Wnt-bead, recruiting it and retaining it at the membrane for a long period (*middle*), or an ESC recruiting a Wnt-bead and releasing it (*right*). Scale bars, 20 μm. Wnt-beads are highlighted by white dashed circle. Time is minutes.

B. Quantification of the percentage of WT ESCs, Wnt pathway KO ESCs, or WT ESCs treated with 10 μM CNQX, contacting Wnt3a-beads or inactive Wnt3a-beads (iWnt3a) at 0 to

12 hours after seeding. Line is centred on mean, error bars are SEM. n = 3, N ≥ 40 cells per timepoint and per n. Stars in box (*right*) indicate statistical significance to WT with Wnt3a-beads, calculated by two-way ANOVA with Tukey multiple comparison test, as follows: ns (*non-significant*, $p > 0.05$), *$p < 0.05$, **$p < 0.01$, ***$p < 0.001$, ****$p < 0.0001$.

C. Graphical representation of the bead retention time in WT ESCs, Wnt pathway KO ESCs, or WT ESCs treated with 10 µM CNQX, contacting Wnt3a-beads or WT ESCs contacting iWnt3a-beads. N ≥ 46 cells/condition are presented as columns. Grey colour indicates cell without beads, Blue colour indicates cell with beads. Time is displayed in the y axis, expressed in minutes.

D. Quantification of the Wnt-bead retention time for cells displayed in **C**. Box indicates median and quartiles, error bars indicate 10-90 percentile, dots are data out of range. Data is pooled approximately evenly from n ≥ 3 independent experiments, total N ≥ 46 cells/condition. Stars indicate statistical significance to WT ESCs contacting Wnt3a-beads, calculated by two-way ANOVA with Tukey multiple comparison tests, as follows: **$p<0.01$, ***$p<0.001$, ****$p < 0.0001$.

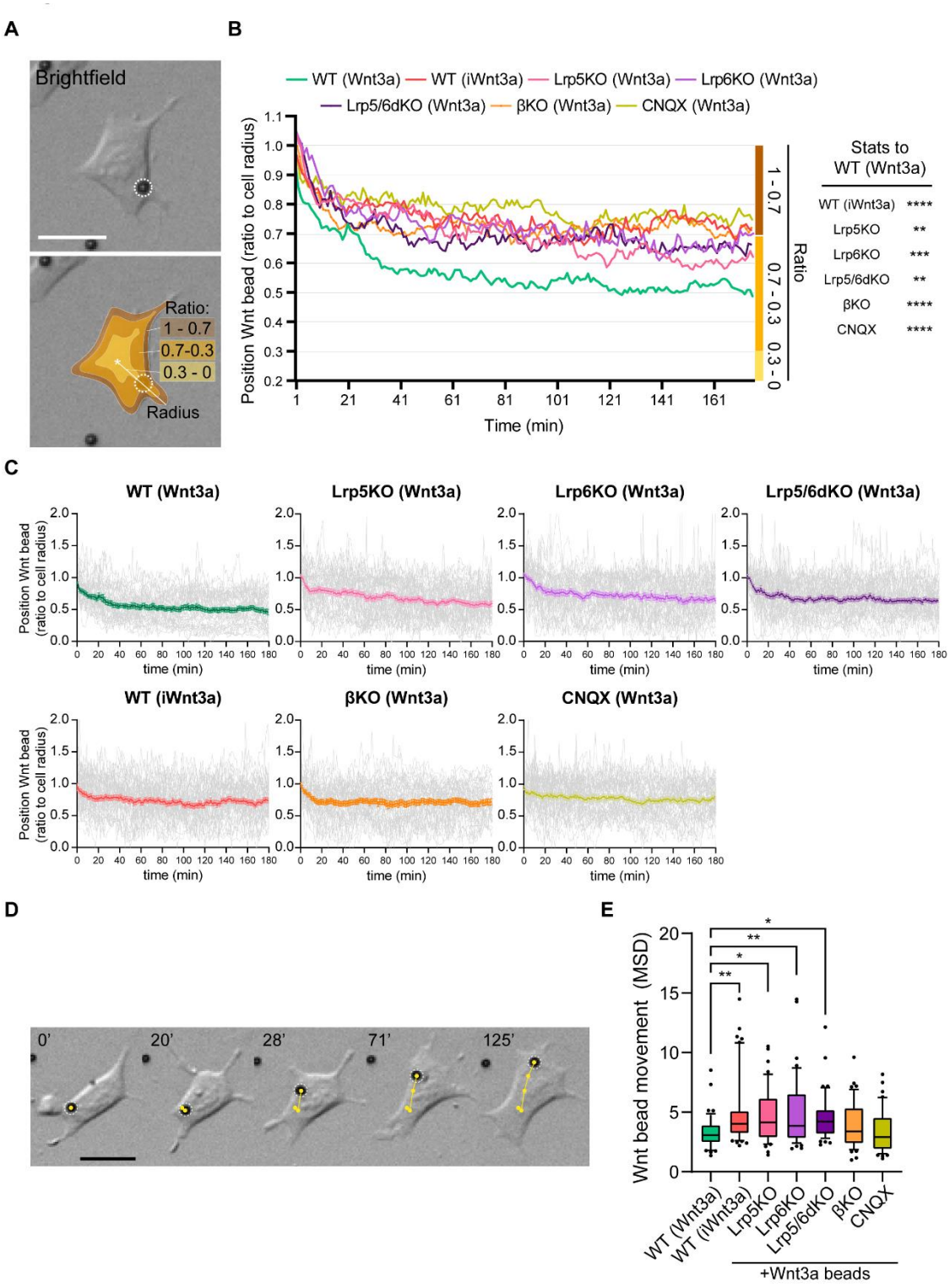

FIGURE 3. Wnt co-receptors and iGluR control Wnt-bead movement and positioning at the membrane

A. Representative brightfield image of an ESC contacting a Wnt3a-bead (*top*). Schematic representation of "membrane" area (1-0.7 ratio of radius, brown), "middle of cell" area (0.7-

0.3 ratio of radius, orange) or "top of cell" area (0.3-0 ratio of radius, yellow), and of the radius used to calculate the areas (white line) (*bottom*). Scale bar, 20 µm.

B. Quantification of Wnt-bead position in the cell, displayed as ratio to cell radius, and measured every minute for 3 hours (180 minutes) after initial Wnt-bead recruitment. Lines are mean per condition. *Right* axis indicates cellular areas, as described in **A**. N ≥ 47 total cells/condition, pooled approximately evenly from n ≥ 3 experiments. Stars indicate statistical significance across time average to WT ESCs contacting Wnt3a-beads, calculated by one-way ANOVA with Tukey multiple comparison test, as follows: ***p < 0.01*, ****p < 0.001, ****p < 0.0001.*

C. Quantification of Wnt-bead position in the cell, displayed as ratio to cell radius, and measured every minute for 3 hours (180 minutes) after initial Wnt-bead recruitment, as summarised in **B**. Coloured lines are mean, grey lines are individual cell tracks, error bars = SEM. N ≥ 47 total cells/condition, pooled approximately evenly from n ≥ 3 experiments.

D. Representative frames of time-course live imaging, displaying an ESC contacting a Wnt bead. Wnt-bead is highlighted with white dashed circle. Yellow track indicates Wnt-beads movement on the cell over time. Scale bar, 20 µm. Time is minutes.

E. Quantification of Wnt-bead movement on the cell, presented as MSD. Bead movement was measured every minute for 3h (180 min) after recruitment in WT ESCs contacting Wnt3a- or iWnt3a-beads, in Wnt pathway KO ESCs contacting Wnt3a-beads or in WT ESCs treated with 10 µM CNQX contacting Wnt3a-beads. Box indicates median and quartiles, error bars indicate 10-90 percentile, dots are data outside 10-90 percentile range. N ≥ 46 total cells/condition, pooled approximately evenly from n ≥ 3 experiments. Stars indicate statistical significance calculated by one-way ANOVA with Tukey multiple comparison, as follows: **p < 0.05*, ***p < 0.01.*

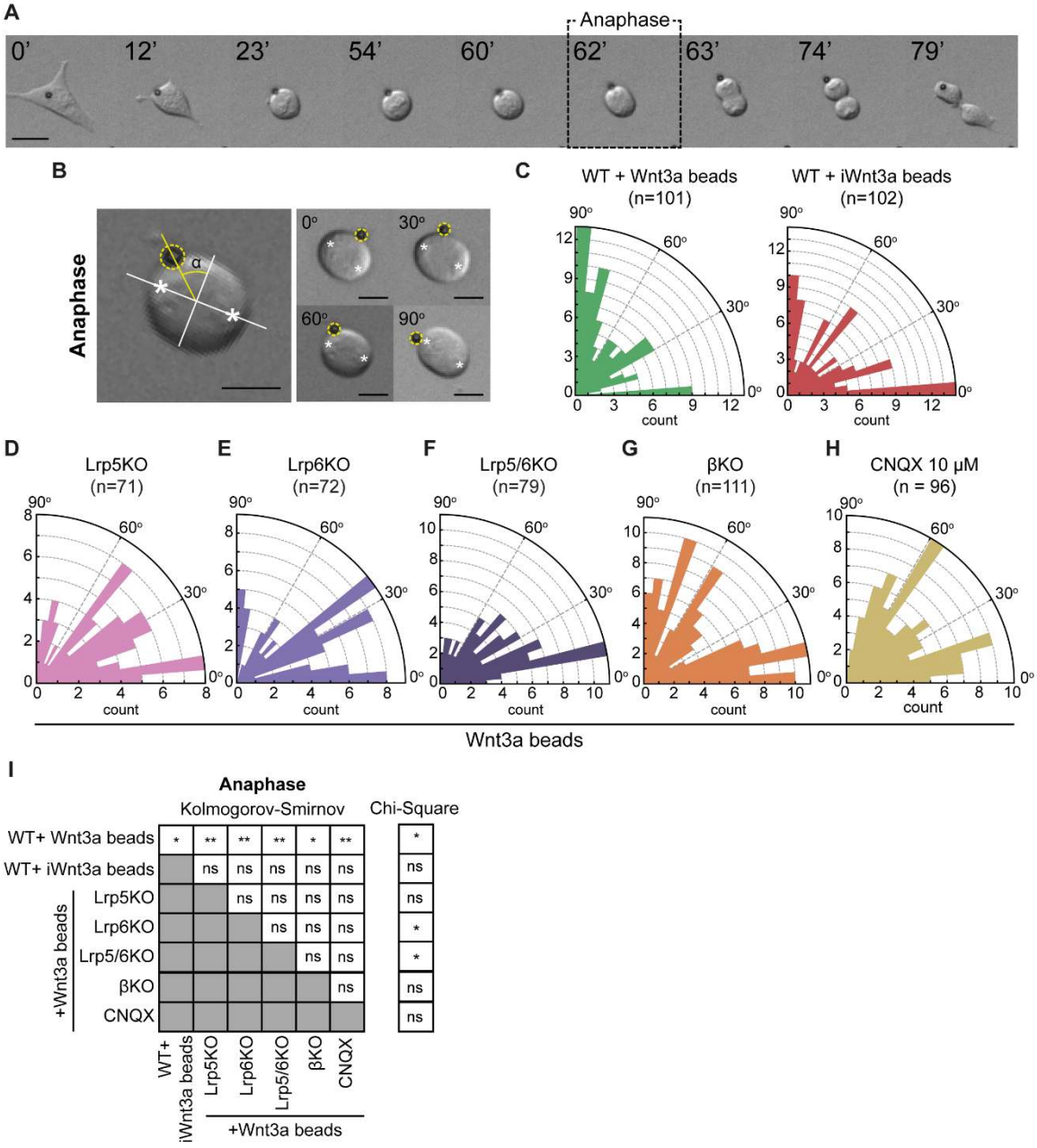

FIGURE 4. Wnt/β-catenin pathway and iGluR activity regulate the orientation of the mitotic spindle

A. Representative frames of a time-course live imaging, displaying an ESCs contacting a Wnt-bead and undergoing an oriented division. Wnt-bead is black sphere. Scale bar, 20 μm. Time is minutes. Dashed box indicates the "Anaphase" timepoint used for spindle orientation analysis.

B. (*Left*) Representative image of the method used for spindle angle measurement relative to Wnt-bead position. Asterisks indicate cell poles used as reference for the measurement. Orthogonal white lines depict major and minor axis, yellow line points to Wnt-bead and limits the angle measured (α). Wnt-bead is highlighted with yellow dashed circle. (*Right*)

Representative images of ESCs dividing with Wnt-beads at different angles (indicated in the figure). Scale bars, 10 μm.

C. Rose-plots depicting the spindle angle at anaphase relative to Wnt-bead in WT ESCs contacting Wnt3a-beads (*left*, green) or iWnt3a-beads (*right*, red). Number of cells (n) is displayed in the figure, pooled approximately evenly from n ≥ 3 experiments.

D – H. Rose-plots depicting the spindle angle at anaphase in Lrp5KO (**D**, pink), Lrp6KO (**E**, purple), Lrp5/6dKO (**F**, dark purple), βKO (**G**, orange) contacting Wnt3a-beads or WT ESCs treated with 10 μM CNQX contacting Wnt3a-beads (**H**, yellow). Number of cells (n) is displayed in the figure, pooled approximately evenly from n ≥ 3 experiments.

I. Statistical comparison of spindle angles between all conditions, at anaphase. (*Left*) Kolmogorov-Smirnov comparison of angle distribution between conditions. (*Right*) Chi-squared comparison of the angles of each condition to a random (n/3: n/3: n/3 for 0°-30°: 30°-60°: 60°-90°) distribution. Stars indicate statistical significance, as follows: ns (*non-significant*, $p > 0.05$), *$p<0.05$, **$p<0.01$.

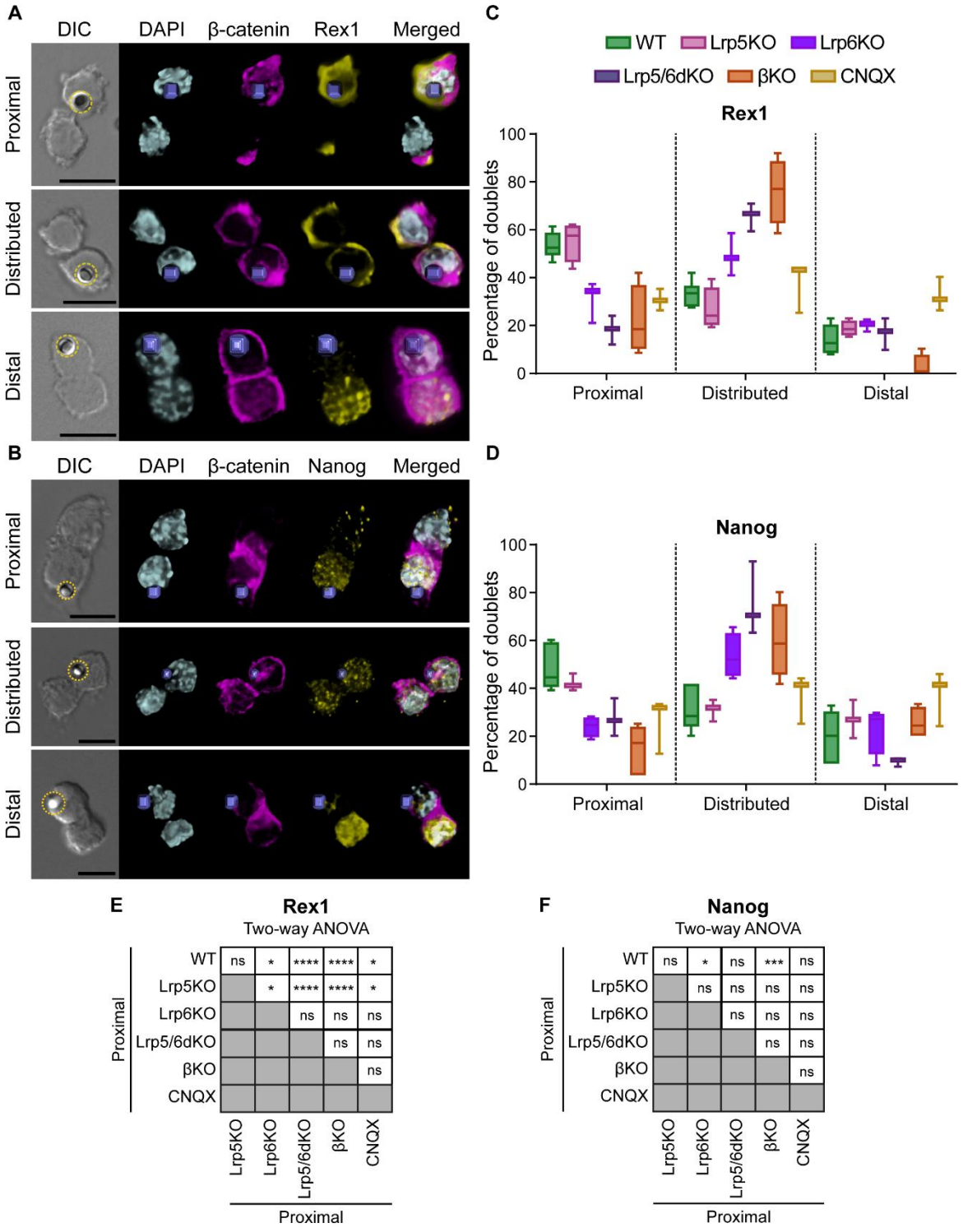

FIGURE 5. β-catenin and Lrp6 and iGluR activity are required for Wnt-mediated asymmetric cellular division

A and B. Representative images of ESC doublets after dividing in contact with a Wnt3a-bead, labelled with antibodies against β-catenin (magenta), Rex1 (**A**, yellow), Nanog (**B**, yellow) or 4′,6-diamidino-2-phenylindole (DAPI, cyan). Images are 3D renderings of mathematically deconvolved raw fluorescent images. DIC is Differential Interference

Contrast. Panels display doublets with higher marker expression in the Wnt-bead contacting cell (*Top*, Proximal), with distributed levels of expression between cells (*Middle*, Distributed) or with higher marker expression in the cell not contacting a Wnt-bead (*Bottom*, Distal). Wnt-bead is highlighted by yellow dashed circle in DIC or reconstructed as purple box in fluorescence images. Scale bars are 20 μm.

C and D. Quantification of the percentage of doublets displaying Proximal, Distributed or Distal Rex1 (**C**) or Nanog (**D**) distribution. n ≥ 3, each with N ≥ 7 doublets. Box indicates median and quartiles, error bars indicate 10-90 percentile.

E and F. Statistical comparison of proximally dividing cells amongst conditions, calculated by two-way ANOVA with Tukey multiple comparison test. Stars indicate statistical significance as follows: ns (*non-significant*, $p > 0.05$), *$p < 0.05$, **$p < 0.01$., ***$p < 0.001$, ****$p < 0.0001$.

CAPTIONS FOR SUPPLEMENTARY MOVIES

Movie 1. Protrusions of WT ESCs. High-quality phase images of WT ESCs generating protrusions. Images were obtained by 3D holotomographic microscopy. Scale bar, 20 μm.

Movie 2. Protrusions of Lrp5KO ESCs. High-quality phase images of Lrp5KO ESCs generating protrusions. Images were obtained by 3D holotomographic microscopy. Scale bar, 20 μm.

Movie 3. Protrusions of Lrp6KO ESCs. High-quality phase images of Lrp6KO ESCs generating protrusions. Images were obtained by 3D holotomographic microscopy. Scale bar, 20 μm.

Movie 4. Protrusions of Lrp5/6dKO ESCs. High-quality phase images of Lrp5/6dKO ESCs generating protrusions. Images were obtained by 3D holotomographic microscopy. Scale bar, 20 μm.

Movie 5. Protrusions of βKO ESCs. High-quality phase images of βKO ESCs generating protrusions. Images were obtained by 3D holotomographic microscopy. Scale bar, 20 μm.